21st Australasian Fluid Mechanics Conference
Adelaide, Australia
10-13 December 2018

Vortical Structures of Laminar Boundary Layer over Convergent-Divergent Riblets with Spanwise Height Variations

F. Xu, S. Zhong and S. Zhang

School of Mechanical, Aerospace and Civil Engineering
University of Manchester, Manchester M13 9PL, UK

Abstract

In this paper, a laminar boundary layer over convergent-divergent riblets with a reduced riblet height in the converging region is investigated experimentally. The flow field in the longitudinal plane and the wall-parallel plane is measured using mono particle image velocimetry (PIV). With a decreased riblet height along the converging line h_{CL}, the intensity of the induced secondary flow over the converging region is significantly reduced, while the flow field characteristics over the diverging region are basically preserved. Detailed analysis on the in-plane flow field provides a deeper understanding of the flow topology of vortical structures. With a spanwise riblet height variation, a weak recirculating secondary flow still exists in the cross-stream plane.

Introduction

The nature-inspired surface pattern of convergent-divergent riblets (referred to as C-D riblets later on) is a new type of spanwise roughness heterogeneity which begins to attract attention more recently. Both vortical structures and the control effect of C-D riblets are inherently different from conventional longitudinal (streamwise) riblets. With large-scale vortical structures induced by the directional spanwise heterogeneity, this roughness pattern is expected to have a broad engineering application prospect in friction drag reduction and flow separation control [4, 6]. To date, there have been several researches on the flow topology of a boundary layer over C-D riblets with uniform riblet height rather than variable riblet height along the spanwise direction. Parameters of C-D riblets, including riblet height, riblet spacing, yaw angle and riblet wavelength, have been studied in several previous studies [5, 2, 7].

An increase in the skin friction drag is observed along the converging line while an opposite effect is obtained along the diverging line [5, 3]. A decrease in riblet height in the converging region, as observed on bird flying feathers, is expected to result in a less intense secondary flow, and consequently a reduction in the skin friction drag in that region. With SEM photos, Chen et al. revealed that the height of the surface roughness of mature pigeon feathers decreases by around three quarters from $130\mu m$ near the feather shaft to $30\mu m$ at the outer fringe [1]. Based on this intriguing characteristic, a spatial-3D configuration is proposed in [2], which has a zero height along the converging line and a linear variation of the riblet height in the spanwise direction. Chen et al. revealed the global drag reduction effect in a fully-developed turbulent pipe flow [2]. A drag reduction of about 20% is obtained for such spatial-3D configuration [2], in contrast to a net drag increase for the pattern with uniform riblet height along the spanwise direction [5].

To date, the influence of a spanwise variation in the riblet height on the flow field is not yet clear. To address this issue, we investigate a laminar boundary layer over C-D riblets with three types of spanwise height variations using mono PIV measurement. The flow field characteristics in both the longitudinal plane and the wall-normal plane are analysed.

Experiment system

Water flume

The experiment is conducted in a $3.64m$ long water flume with a $305mm \times 305mm$ cross-section. A laminar boundary layer is generated over a $6mm$ thick flat plate which is submerged horizontally in the water flume, and a small negative inclination angle is applied to ensure an attached flow from the $1:5$ elliptical leading edge. The free-stream velocity is $0.1m/s$, and the turbulence intensity outside the boundary layer is around 0.2%. The velocity profile of the baseline laminar flow is aligned with the theoretical Blasius profile (not shown here for brevity). The Reynolds number $Re_x = U_\infty x/\nu$ at the measurement section is around 7×10^4.

Convergent-divergent riblets with spanwise height variation

The schematic diagram of C-D riblets with triangular riblet teeth is shown in figure 1, and parameters of C-D riblets are listed in table 1. The riblet section starts at $x = 0.67m$ from the leading edge of the flat plate. To investigate the effect of spanwise riblet height variation, three types of C-D riblet patterns are designed, as shown in figure 2. The riblet height along the diverging line $h_{DL} = h$ is $2.4mm$ for all three cases. The riblet height in the longitudinal plane along the converging line h_{CL}, as indicated in figure 2, has three values of $2.4mm$ (uniform height), $1.2mm$ (half height) or 0 (zero height), and a linear variation of the riblet height is designed in the spanwise direction. The smooth wall levels with half of the adjacent riblet height, i.e. the protrusion height h_p is $h_{DL}/2$ ($h_{CL}/2$) for the wall surface adjacent to the diverging line (converging line). As shown in figure 1, the streamwise, wall-normal and spanwise directions correspond to axes x, y and z, which are normalised by s_x ($6mm$, riblet spacing projected in x direction), δ_{FP} ($12.7mm$, $99\%U_\infty$ boundary layer thickness of the flat plate) and Λ ($45mm$, riblet wavelength) respectively.

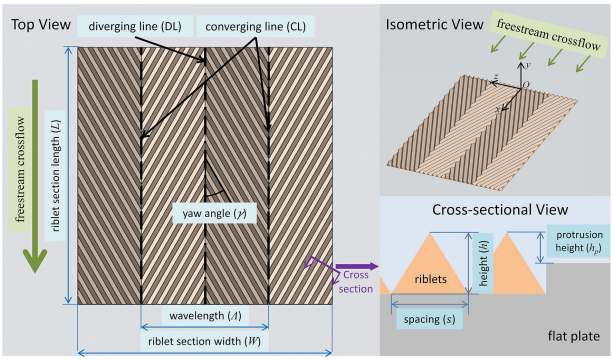

Figure 1: Schematic diagram of C-D riblets parameters [7]. The region close to the converging/diverging line is referred to as the converging/diverging region.

Parameter	Value	Parameter	Value
Λ	$45mm$	L	$90mm$
s	$3.0mm$	W	$90mm$
h_{DL} (h)	$2.4mm$	γ	30°

Table 1: Parameters of C-D riblets.

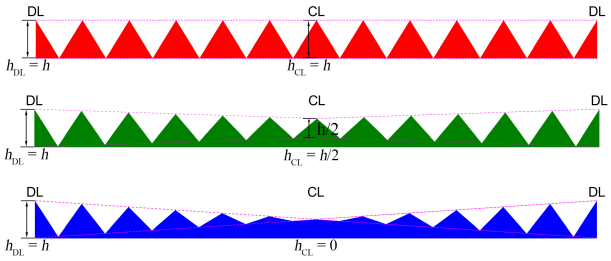

Figure 2: Cross-sectional view in the cross-stream (y-z) plane of C-D riblets with (a) $h_{CL} = h$, (b) $h_{CL} = h/2$, (c) $h_{CL} = 0$. Dashed lines indicate a linear variation of the riblet height along the spanwise direction.

Particle Image Velocimetry System

The mono PIV system from TSI is composed of a New Wave Solo-PIV 120 laser generator, a laser pulse synchroniser (Model 610036) and a CCD camera (4 Mega pixels). The longitudinal (x-y) measurement plane covers the whole riblet section. The distance between the wall-parallel (x-z) measurement plane and the smooth wall surface is $3mm$. The laser pulse time interval is $6ms$ in the longitudinal plane or $8ms$ in the wall-parallel plane, and the width of the laser light sheet is around $1mm$. A total of 1250 image pairs are captured with an acquisition rate of $2Hz$ to ensure convergence of the time-averaged results.

In these measurement planes, PIV image pairs are processed using $64 \times 24/24 \times 24$ as the first/final interrogation area with a 50% overlap. Table 2 lists parameters of the field of view and the spatial resolution of velocity vectors. The expanded uncertainties in the time-averaged velocity components, i.e. 95.4% possibility of having true value within the uncertainty bound, are $0.05\%U_{\infty}$ in the longitudinal plane and $0.28\%U_{\infty}$ in the wall-parallel plane.

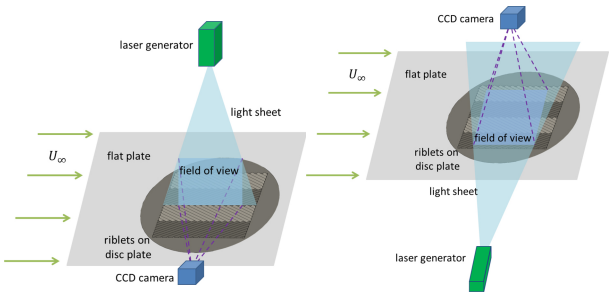

Figure 3: Mono PIV arrangement [7] in (a) the longitudinal plane, (b) the wall-parallel plane.

Plane	Field of view	Spatial resolution
Longitudinal (x-y)	117.32×88.19	0.60×0.60
Wall-parallel (x-z)	137.29×103.20	0.70×0.70

Table 2: Parameters of mono PIV datasets (unit: mm^2).

Results and analysis

Figure 4 compares the distribution of time-averaged streamwise velocity contours of three types of spanwise height variations. For the uniform riblet height, the local streamwise velocity decreases rapidly in the near-wall region in figure 4(a). For $h_{CL} = h/2$, similar distributions of the velocity components are observed in figure 4(b), while the magnitudes are significantly smaller. For $h_{CL} = 0$, the distribution of the streamwise velocity in figure 4(c) resembles the undisturbed boundary layer over a flat plate.

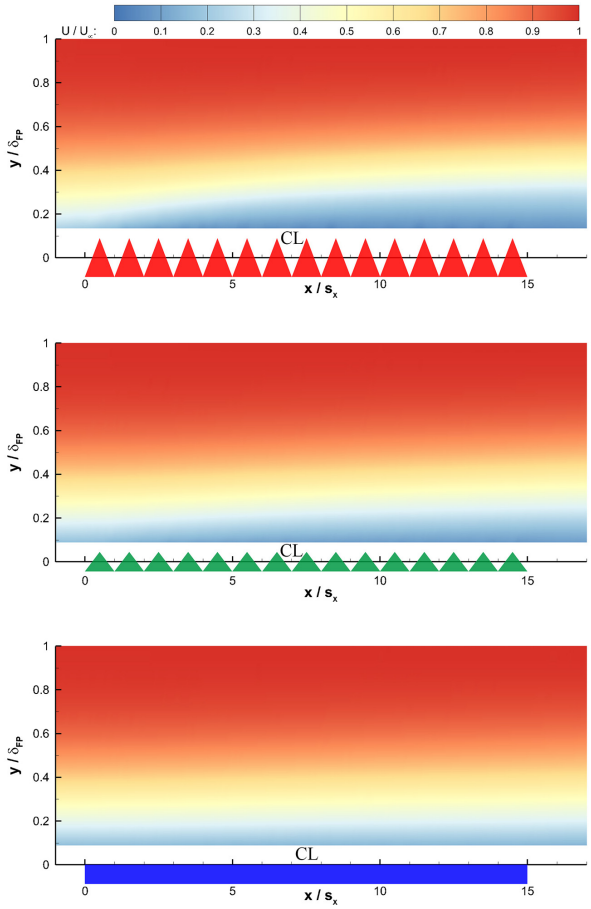

Figure 4: Time-averaged streamwise velocity over C-D riblets with (a) $h_{CL} = h$, (b) $h_{CL} = h/2$, (c) $h_{CL} = 0$.

Figure 5 compares the time-averaged streamwise velocity profiles at multiple streamwise stations over the converging line. The velocity profiles over the diverging line for three cases present only slight differences compared with those over the converging line, and thus are not shown here for the sake of brevity. Over the converging line, the streamwise velocity profile continues to evolve as a result of the progressive decrease in the streamwise velocity in the near-wall region and the gradual spreading of this region of reduced velocity towards the edge of the boundary layer. A decrease in h_{CL} leads to a narrower affected region in the wall-normal direction. The streamwise velocity profiles of the $h_{CL} = 0$ case resemble those over the flat plate, indicating ignorable flow disturbances over the converging region.

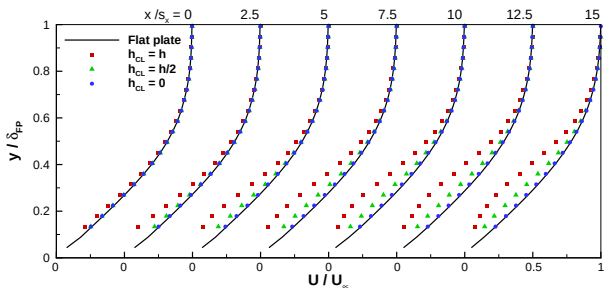

Figure 5: Time-averaged streamwise velocity profiles in the longitudinal plane along the converging line.

Figure 6 reveals the streamwise variations of the displacement thickness and the shape factor of the boundary layer along the converging line. Those parameters of a flat plate boundary layer are also included as a reference (black diamond). The boundary layer displacement thickness (δ_1) representing modification to the velocity shape is less sensitive to the free-stream velocity than the $99\%U_\infty$ boundary layer thickness (δ), which makes it more suitable to represent the changes in the local streamwise velocity within the boundary layer. Upstream of the riblet section ($x < 0$), a tiny increase in the displacement thickness is observed, which is caused by the blocking effect of the riblets above the smooth wall surface. In the region over the converging line, a lower local streamwise velocity leads to increased values of the displacement thickness and the shape factor than those of the baseline boundary layer. With an increased value of h_{CL}, a more substantial increase in δ_{CL} and H is observed, indicating that more low-velocity fluid is accumulated at the bottom of the boundary layer.

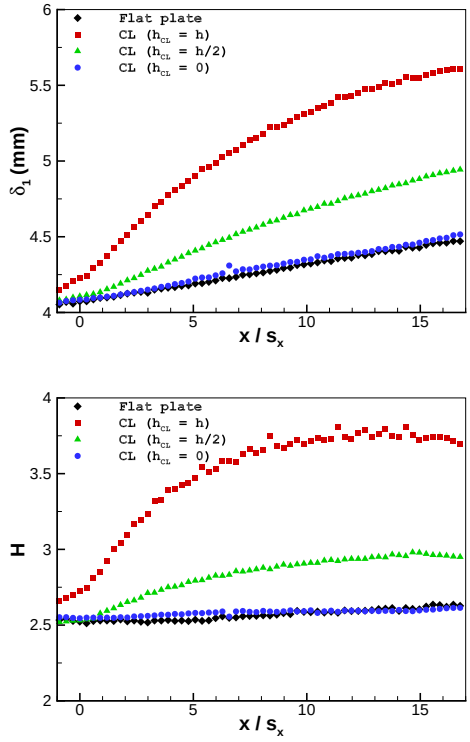

Figure 6: Comparison of (a) boundary layer displacement thickness δ_1, (b) shape factor H.

Figure 7 shows contours of the time-averaged induced streamwise velocity in the wall-parallel plane. Based on figure 5, the streamwise velocity in the same wall-parallel plane over the flat plate is subtracted to reveal the induced velocity contour. In figure 7(a), a concentrated stripy zone with velocity defect (blue colour) is observed over the converging region, while stripy zones with velocity excess (red colour) are obtained over the diverging region. In comparison, with a reduced h_{CL} in figure 7(b) and figure 7(c), the intensity of induced streamwise velocity weakens over the converging region, while stripy shapes still exist over the diverging region.

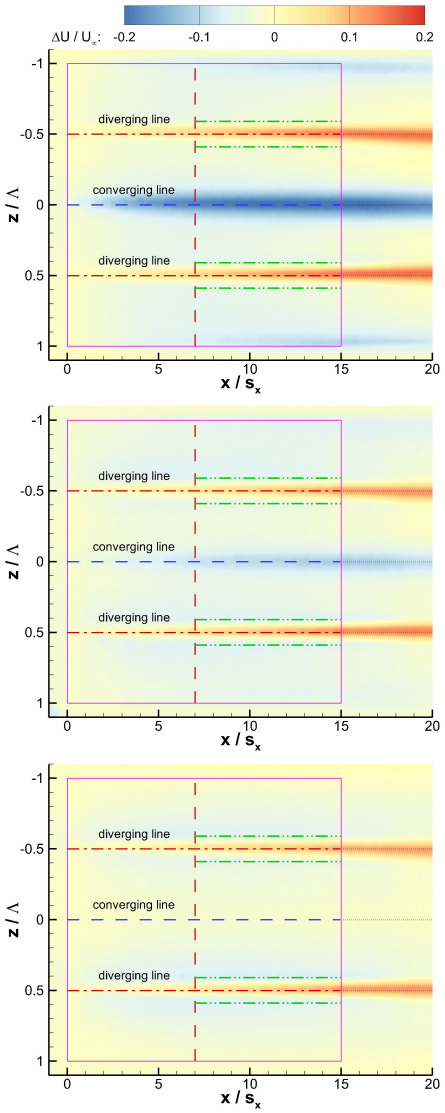

Figure 7: Time-averaged induced streamwise velocity over C-D riblets with (a) $h_{CL} = h$, (b) $h_{CL} = h/2$, (c) $h_{CL} = 0$ in the wall-parallel plane.

Figure 8 shows contours of the time-averaged spanwise velocity in the wall-parallel plane. Based on the findings in [7], the development of a boundary layer over C-D riblets with uniform riblet height can be divided into a developing stage followed by a developed stage, with their separation locates at $x \approx 7s_x$. In figure 8(a), the distribution of the spanwise velocity indicates a distinct difference between these two stages. In the developing stage ($x < 7s_x$), the sign of the spanwise velocity component indicates a spanwise flow from the diverging line to the converging line, which is aligned with the spanwise direction of riblet valleys. In this stage, no recirculating secondary flow is formed in the cross-stream plane. The fluid above the wall surface in the wall-parallel plane follows the fluid at a lower level

which evolves along riblet valleys, as indicated in figure 9(a). In the developed stage ($x > 7s_x$), a spanwise flow opposite to the direction of riblet valleys is observed, which indicates the existence of a weak recirculating secondary flow in the cross-stream plane. The wall-parallel measurement plane in the present experiment is above the vortex centre of the recirculating secondary flow, and thus a reversed spanwise flow exists in the plane, as depicted in figure 9(b). With a decreased value of h_{CL} in figure 8(b) and figure 8(c), the weak recirculating secondary flow still exists in the cross-stream plane, although the intensity is expected to be lower.

Further analysis on the local characteristics of the time-averaged spanwise velocity in figure 8(a) also provides a deeper understanding on the flow topology over C-D riblets (refer to FIG.9 in [7]). Close to the diverging line, there exist a few spotted zones which indicate local spanwise flow away from it. These spotted zones can be interpreted as the footprints of the fluid evolving inside riblet valleys in the wall-parallel plane. The streamwise distance between adjacent spotted zones is s_x, with each spotted zone corresponds to one riblet valley. The existence of these spotted zones indicates that the vortical structures in the cross-stream plane may vary slightly at different streamwise stations. Since the value of h_{CL} mainly affects the flow field characteristics over the converging region, the spotted zones close to the diverging line can still be observed in figure 8(b) and figure 8(c). Considering that the induced streamwise velocity is one to two orders of magnitude larger than the spanwise component, these spotted zones are not reflected in the contours of the streamwise velocity.

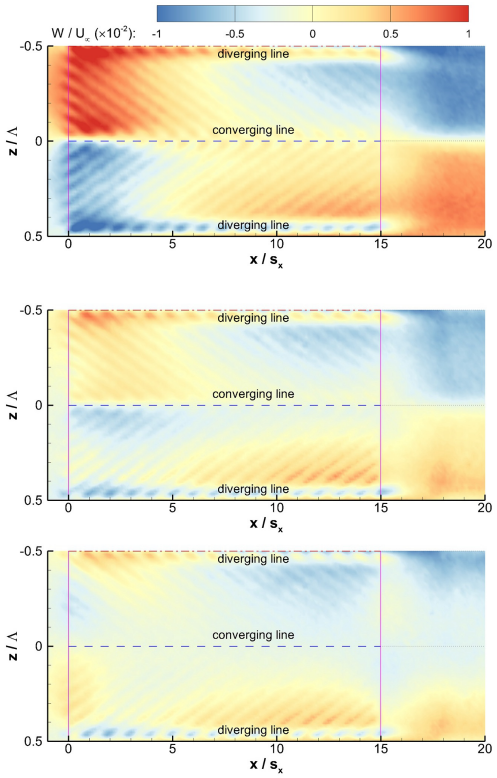

Figure 8: Time-averaged spanwise velocity over C-D riblets with (a) $h_{CL} = h$, (b) $h_{CL} = h/2$, (c) $h_{CL} = 0$ in the wall-parallel plane.

Conclusion

A laminar boundary layer over a spanwise roughness pattern of C-D riblets with a spanwise height variation, i.e. a reduced

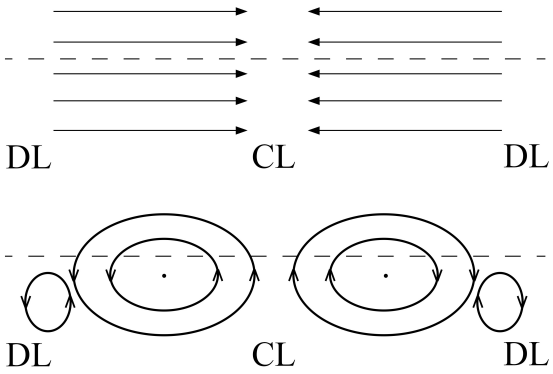

Figure 9: Schematic of the spanwise velocity and the relative position of the wall-parallel plane in the cross-stream plane in (a) the developing stage, (b) the developed stage. The dashed line indicates the station of the wall-parallel plane.

riblet height in the converging region, is analysed in multiple measurement planes in this paper. A reduced h_{CL} value leads to a less intense secondary flow, which includes a thinner boundary layer and a weaker induced streamwise velocity over the converging region. The induced flow field over the converging region is ignorable when the riblet height of this region is zero. In contrast, the flow field characteristics present only slight changes over the diverging region.

Acknowledgements

The authors would like to acknowledge the warm technical supports from the workshop technicians at the School of Mechanical, Aerospace and Civil Engineering.

References

[1] H. Chen, F. Rao, X. Shang, D. Zhang, and I. Hagiwara. Biomimetic drag reduction study on herringbone riblets of bird feather. *Journal of Bionic Engineering*, 10(3):341–349, 2013.

[2] H. Chen, F. Rao, X. Shang, D. Zhang, and I. Hagiwara. Flow over bio-inspired 3D herringbone wall riblets. *Experiments in Fluids*, 55:1698, 2014.

[3] Kevin, J. P. Monty, H. L. Bai, G. Pathikonda, B. Nugroho, J. M. Barros, K. T. Christensen, and N. Hutchins. Cross-stream stereoscopic particle image velocimetry of a modified turbulent boundary layer over directional surface pattern. *Journal of Fluid Mechanics*, 813:412–435, 2017.

[4] K. Koeltzsch, A. Dinkelacker, and R. Grundmann. Flow over convergent and divergent wall riblets. *Experiments in Fluids*, 33(2):346–350, 2002.

[5] B. Nugroho, N. Hutchins, and J. P. Monty. Large-scale spanwise periodicity in a turbulent boundary layer induced by highly ordered and directional surface roughness. *International Journal of Heat and Fluid Flow*, 41:90–102, 2013.

[6] B. Nugroho, Kevin, J. Monty, N. Hutchins, and E. Gnanamanickam. Roll-modes generated in turbulent boundary layers with passive surface modifications. In *52nd Aerospace Sciences Meeting*, Reston, Virginia, 2014. American Institute of Aeronautics and Astronautics.

[7] F. Xu, S. Zhong, and S. Zhang. Vortical structures and development of laminar flow over convergent-divergent riblets. *Physics of Fluids*, 30(5):051901, 2018.